Structural and spectroscopic characterization of CeO2-TiO 2 mixed oxides

Journal Name

Dynamic Article Links ►

Cite this: DOI: 10.1039/c0xx00000x

www.rsc.org/xxxxxx

ARTICLE TYPE

Structural and spectroscopic characterization of CeO_2-TiO_2 mixed oxides.

Chiara Gionco,[a] Maria Cristina Paganini,[a] Stefano Agnoli,[b] Askia Enrico Reeder[b] and Elio Giamello*[a]

Received (in XXX, XXX) Xth XXXXXXXXX 20XX, Accepted Xth XXXXXXXXX 20XX

DOI: 10.1039/b000000x

Mixed CeO_2-TiO_2 systems have been synthesized using the sol-gel technique in a symmetric range of nominal compositions (0.1, 0.5, 0.9 CeO_2 molar fraction respectively). The solid materials have been characterised using a variety of diffractometric and spectroscopic techniques. The intimate contact between the two components during the synthesis leads to heterogeneous systems which are based on the presence, beside the two individual oxide phases, of a mixed phase of a cerium titanate ($Ce_2Ti_2O_7$, pyrochlore structure) which contains Ce^{3+} ions imparting particular optical properties to the solid (pronounced red shift with respect to the band gap transition of the two oxides). Ce^{3+} ions are present at the surface of the systems together with tetravalent Ce and Ti ions. The mixed solids can be reduced by annealing under vacuum and, upon reoxidation in mild conditions with O_2, form superoxide species adsorbed on Ce^{4+} which have, as already reported for low loading CeO_2-TiO_2 systems, peculiar spectroscopic properties with respect to superoxide adsorbed on bare cerium dioxide.

Introduction

Metal oxides are strategic systems for modern material science not only for their well-known structural properties but, in particular, for their applications in a very high number of sophisticated devices as functional materials. The research in the field of metal oxides is therefore continuously searching for new systems with stimulating and unprecedented properties. This can be done in several ways including the systematic study of complex mixtures of simple oxides. Two, or more, metal oxides can interact in principle in several ways like, for instance, the formation of new compounds, the formation of solid solutions in particular compositional ranges or the simple formation of solid-solid interfaces constituting a heterojunction between two non-miscible phases.

The system involving cerium dioxide and titanium dioxide has been the object of some investigations in the past essentially because the two individual oxides have so many interesting properties and consequent applications, that the exploration of mixed systems is expected to produce promising results[1-4].

Cerium dioxide is well known because of its redox properties allowing easy transitions between oxidized and reduced states, depending on the external conditions. Oxygen storage capacity makes ceria suitable for several applications such as those in automotive three way catalysts[5-7] and, in general, in oxidation catalysis[8-13]. Cerium dioxide is also used as sensor[14, 15], in fuel cell technology as a solid state electrolyte[16, 17], and even in cosmetics[18]. The oxygen storage (and release) in ceria seems to be favoured by its fluorite structure. In fact oxygen ions in such a crystal lie in parallel planes allowing an efficient oxygen diffusion in a network of oxygen vacancies favouring the oxidative action of the solid. By the way the oxygen storage capacity (OCS) is greatly enhanced when Zr is introduced in to the cubic ceria structure and in particular upon formation of phases with pyrochlore structure such as $Ce_2Zr_2O_7$ (*vide infra*)[19-21]. The strong optical absorption around 400nm of cerium dioxide (with a weak tail in the visible range capable of imparting a pale yellow colour to the material) has also stimulated studies devoted to the use of this material as a possible photocatalyst[22].

Titanium dioxide has been widely studied in the last few decades because of its photochemical and photophysical properties[23-25]. This oxide, in fact, is a component of photovoltaic devices (DSSC, dye-sensitized solar cells[26]) and is an active photocatalyst commonly used in several reactions of environmental interest[27]. TiO_2 exists in three crystallographic forms: rutile, anatase and brookite all characterized by octahedrally coordinated Ti^{4+} ions. Although rutile is the most stable phase, anatase shows higher activity in photochemical and photocatalytical phenomena.

In the present paper we report an investigation on CeO_2-TiO_2 (ceria-titania) mixed oxide systems prepared using the sol-gel technique and having high loadings of CeO_2 (from 10% to 90% by mol), at variance with analogous systems consisting in low amounts of ceria dispersed on TiO_2 surface, which have been investigated in the past[28-32]. The sol-gel technique, due to the intimate mixture of the various components in the starting liquid phase, is, among the possible synthetic routes, one of the more suited to favour a deep interaction between the two phases.

Despite the previous activity concerning this system, some of which devoted to improve the thermal stability of CeO_2[30, 31, 33-36], several questions about its structural and electronic features have not yet found a clear answer. For instance the insertion of cations of one type (Ce^{4+}or Ti^{4+}) into the lattice of the other oxide (TiO_2 or CeO_2) is a questioned point in the literature. The two oxides

are basically immiscible due to the different crystal structure and to the different cationic size (Ce^{4+} 0.92-0.97 Å; Ce^{3+} 1.14 Å, Ti^{4+} 0.61 - 0.68 Å). However some authors[1, 2, 37-39] assert that, while the insertion of cerium in the TiO_2 lattice is unlikely because of the different size, the insertion of weak concentrations of Ti^{4+} in CeO_2 should be instead possible. On the contrary other authors[3, 29] claim that cerium ions can actually enter into the titania lattice[4, 40] indicating a quite relevant value (5mol%) for the maximum concentration. In general, however, most authors agree in describing the coexistence of the two oxides phases and the formation at the interface of small domains of mixed phases.

The materials synthesized for the present investigation were characterized by a variety of techniques including X-ray Diffraction (XRD), N_2 adsorption to evaluate BET surface area, diffuse reflectance UV-Vis spectroscopy, μ-Raman spectroscopy, transmission electron microscopy (TEM with EDS), x-ray photoemission spectroscopy (XPS) and electron paramagnetic resonance (EPR). Aim of this investigation was a deep insight into the properties of this mixed oxide. We focussed our attention mainly on the features of the oxide-oxide interface, on the optical properties of the system and, due to the high CeO_2 content, on its reactivity towards oxygen. As it will be seen in the following, the features of the mixed systems, prepared in this way, are original and not amenable to those of a simple mixture of the two oxides.

Materials and Methods

Preparation of samples

All reactants employed in this work were purchased by Aldrich and used without any further purification treatment. In particular the cerium nitrate was free from other rare earth elements impurities.

Mixed Ti-Ce oxides were prepared via sol-gel synthesis following the procedure described by Fang et al[2]. For each sample a solution A was prepared stirring 10 g of $Ti(OC_4H_9)_4$, 3 ml of CH_3COOH and 40 ml of C_2H_5OH. The pH of this solution was adjusted to 2.3÷2.7 using HNO_3. Solution B was prepared with a stoichiometric amount of $Ce(NO_3)_3{\cdot}6H_2O$, 3 ml of distilled water and 20 ml of C_2H_5OH. Solution B was added dropwise to solution A while stirring, until a stable sol was formed. This sol has been aged in air until the formation of a gel, then dried at 343K for 72 hours. Finally the powder was calcined at 723 K in air for 2 hours.

The concentrations of the three mixed oxides prepared with the described procedure were 10%, 50% and 90% molar in CeO_2: these materials will be hereafter labeled as CT10, CT50 and CT90, respectively.

Some properties of these mixed oxides were compared with those of pure TiO_2 (anatase polymorph) prepared using the same method (starting from $Ti(OC_3H_7)_4$, C_3H_7OH and distilled water) and with those of a sol-gel prepared (starting from $Ce(OC_3H_7)_4$) CeO_2.

Characterization of samples

Powder X-rays diffraction (XRD) patterns were recorded with a PANalytical PW3040/60 X'Pert PRO MPD using a copper K_α radiation source (0.154056 nm). The intensities were obtained in the 2θ ranges between 20° and 70°. The X'Pert High-Score software was used for data handling. The MAUD 2.26[41] software was used for Rietveld refinement. To determine the instrumental broadening, the pattern obtained by a well, crystallized Silicon standard (crystallite size = 1 μm) was used.

The surface area measurements were carried out on a Micromeritics ASAP 2020/2010 using the Brunauer-Emmett-Teller (BET) model on the N_2 adsorption measurement. Prior to the adsorption run, all the samples were outgassed at 573K for 3h.

Micro-Raman (μ-Raman) spectra were recorded on a Jobin Yvon LabRam HR800 spectrometer, equipped with a He-Ne laser (632.8 nm), connected to an Olympus BX41 microscope.

TEM analysis of the powder samples deposited on a copper grid was performed using a Jeol JEM 3010 (300kV) microscope equipped with a EDS detector by Oxford Instruments.

The UV-Vis absorption spectra were recorded using a Varian Cary 5 spectrometer, coupled with an integration sphere for diffuse reflectance studies, using a Carywin-UV/scan software. A sample of PTFE with 100% reflectance was used as reference.

Electron Paramagnetic Resonance (EPR) spectra, recorded at room temperature and at liquid nitrogen temperature, were run on a X-band CW-EPR Bruker EMX spectrometer equipped with a cylindrical cavity operating at 100 kHz field modulation and computer simulation of the spectra were obtained using the SIM32 programme developed by Prof. Sojka (Jagellonian University, Cracow, Poland[42]).

The XPS measurements were carried out in an ultrahigh vacuum system equipped with a VG MkII Escalab electron analyzer, working at a base pressure of 10^{-10} mbar. Photoemission spectra were taken at room temperature in normal emission using a non monochromatized Al/Mg twin anode x-ray source. Powder samples were suspended in bidistilled water and drop casted on high purity copper foils. After drying in air, the obtained films were introduced in the ultrahigh vacuum chamber and outgassed overnight. The charging observed during measurements was corrected using adventitious carbon as internal reference.

RESULTS AND DISCUSSION

X-Ray Diffraction patterns and Transmission Electron Microscopy

XRD patterns of the samples investigated in this work are shown in figure 1. The diffraction peaks of the mixed materials are broad in comparison with those of bare ceria with a maximum for CT50.

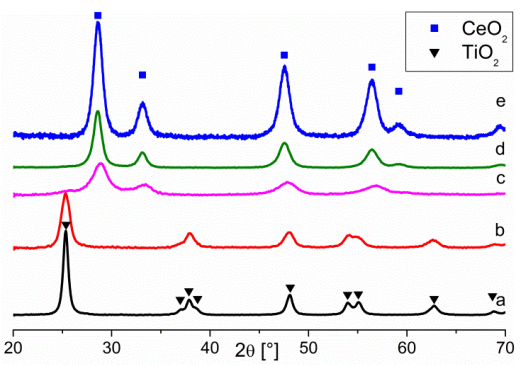

Fig. 1 . XRD of CeO_2/TiO_2 mixed oxides: (a) TiO_2 (sol-gel); (b) 10% mol CeO_2, CT10;(c) 50% mol CeO_2, CT50; (d) 90% mol CeO_2, CT90; (e) CeO_2

Table 1 Cell parameters, weight percentage and crystallite size obtained from Rietveld refinement of the XRD patterns of bare and mixed Ce-Ti oxides. R_{wp} is the weighted residual error, *a* and *c* are lattice parameters, %mol is the molar percentage of the cerium dioxide phase, d is the average crystallite size. S_{BET} is the surface area derived from nitrogen adsorption measurements.

	R_{wp} [%]	Cerium dioxide			TiO_2-Anatase			S_{BET} [m^2/g]
		% mol	*a* [Å]	d [nm]	*a* [Å]	*c* [Å]	d [nm]	
TiO_2	7.84	0			3.785±0.002	9.500±0.009	22±1	85±4
CT10	7.52	10±2	5.41	~2	3.792±0.003	9.503±0.003	14±1	130±7
CT50	9.00	54±8	5.404±0.002	6±1				75±4
CT90	6.94	92±3	5.409±0.008	13±1				83±4
CeO_2	2.73	100.0	5.412±0.002	12±1				50±3

Because of the high Ce atomic mass the peaks of cerium dioxide dominate the diffractograms of CT90 and CT50 samples (in this latter the main TiO_2 peak only, at 2θ=26°, is barely visible). However the sample containing 10 mol% of ceria (CT10) essentially shows peaks corresponding to the TiO_2 anatase phase indicating, for this sample, a strong dispersion of cerium dioxide.

Table 1 lists the relative abundance of the two phases, the lattice parameters and the average crystals size calculated using a Rietveld refinement. The specific surface areas measured by the BET method are also listed.

The lattice parameters of ceria and anatase phases in the mixed materials are not significantly modified with respect to those of the bare oxides. This suggests, also considering the large difference in ionic radius for the two cations involved, that the presence of solid solutions in mixed samples is rather unlikely.

From XRD data analysis it shows up that the average crystallites size decreases moving from the bare oxides to the mixed samples, the smallest crystallites being observed in the case of the 50% molar sample. All prepared powders are made up by nanocrystals. The higher B.E.T. surface area (130 m^2/g) is obtained for CT10. In general all mixed oxides show a higher surface area with respect to that of bare ceria.

Figure 2 reports the atomic maps obtained by EDS for the mixed samples. The maps show a good spatial dispersion of the two metals. The difference in brightness only depends on the time employed for the measurement. In conclusion, on the basis of the structural results here reported, we can state that the two oxides mix up together quite efficiently.

μ-Raman Spectroscopy

The μ-Raman technique was used to further investigate the phase distribution into the mixed samples. Both ceria and titania, in fact, have a good response in Raman spectroscopy, and their typical peaks are observed in distinct spectral regions with limited reciprocal interference. μ-Raman analysis has, furthermore, a good spatial resolution. Therefore, to check the homogeneity of the materials, five acquisitions in different regions were performed for each sample.

The spectra obtained are shown in figure 3. The left hand side of figure 3 reports a typical spectrum for the more homogeneous samples here considered (CT10, CT90), while, on the right hand side, the spectroscopic response in five different points of CT50 is reported to check the spatial distribution of the various phases in this quite heterogeneous material. The Raman spectrum of cerium dioxide shows a main peak at 466 cm^{-1} (Fig.3a). Actually for a fluorite structure like that of CeO_2, six degenerated Raman active [F_{2g}] modes are expected[2, 36, 43-46]. The TiO_2 spectrum (Fig.3d) shows bands at 150, 199, 396, 511, 633 cm^{-1}, congruent to what reported in the literature for the anatase phase[2, 36, 43, 44].

The results in figure 3A for CT10 and CT90 are in agreement with those derived from XRD analysis (Fig.1, Table 1) as the former sample mainly consists of anatase, while the second one is essentially based on the ceria phase, a relatively minor peak only, related to anatase, being visible at 150cm^{-1}.

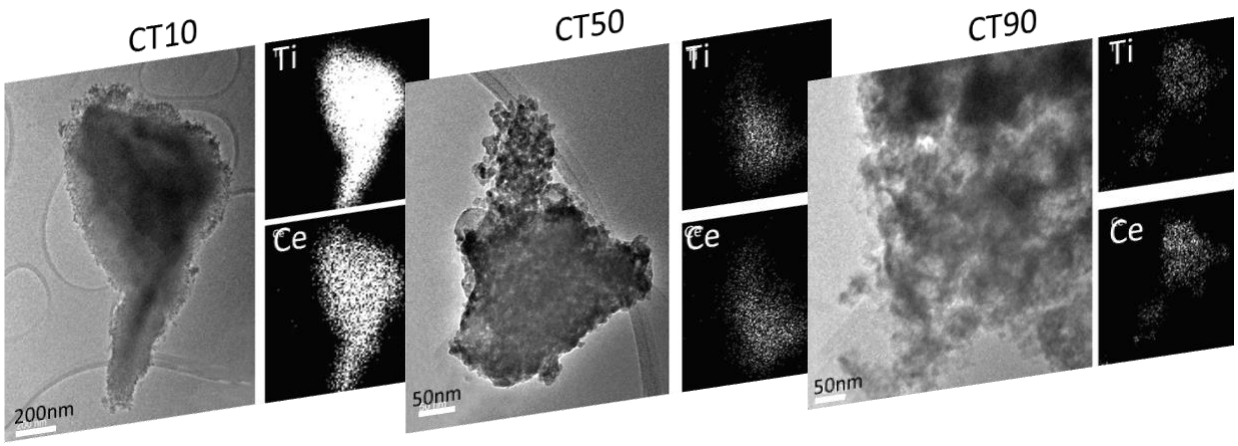

Fig. 2 TEM images of crystal aggregates and related EDS atomic maps of Ti (upper picture) and Ce (lower picture) for CT10, CT50, CT90.

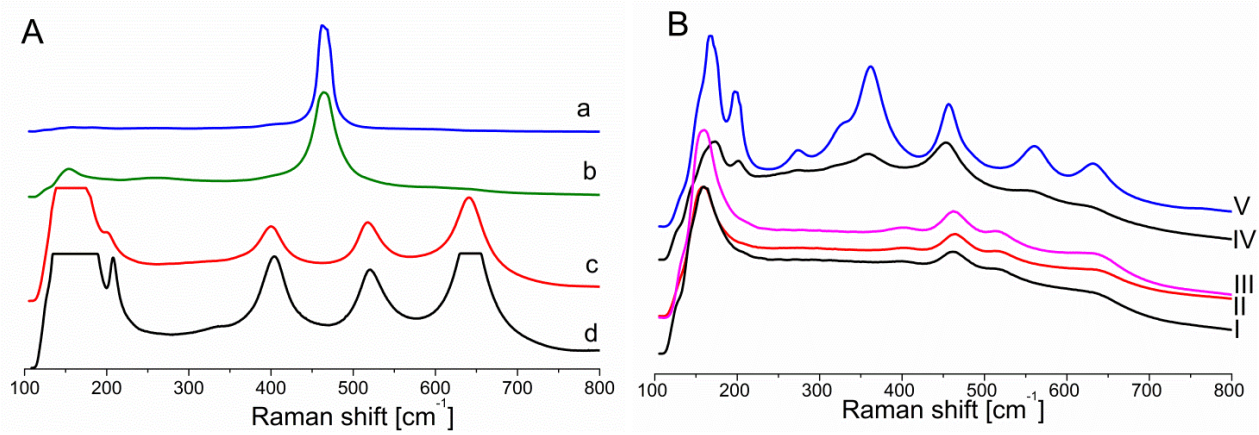

Fig. 3 A) μ-Raman spectra of: CeO_2 (a), CT90 (b), CT10 (c), TiO_2 (d). B) spectra obtained for CT50 in different points of the sample.

CT50 sample is quite inhomogeneous as shown by the spectra grouped in figure 3B. Three of them (from I to III) in fact show the typical bands of ceria and anatase, which are thus both present into the material, while the last two traces (IV and V) show the onset of a new set of lines at 168, 197, 275, 326, 362, 456, 560, 631 cm^{-1} that are assigned to the cerium titanate $Ce_2Ti_2O_7$ phase[44]. The presence of this phase, not detected by XRD for reasons discussed in the following, indicates that a strong interaction has occurred between ceria and titania into the mixed material.

Diffuse Reflectance UV-Vis Spectroscopy.

UV-Vis DR spectra obtained from the mixed oxides are shown in figure 4 where they are compared with the spectra of bare TiO_2 (Fig.4a), bare CeO_2 (4c) and with that of an equimolar mechanical mixture of the two oxides obtained by gentle and prolonged mixing of the two powders (4b).

All three mixed oxides show a net red shift in the main optical transition with respect to the pure oxides and their mechanical mixture indicating that the sol gel method adopted for preparation favours an intimate interaction of the two components and that, additionally, this interaction imparts peculiar optical properties to the mixed solids.

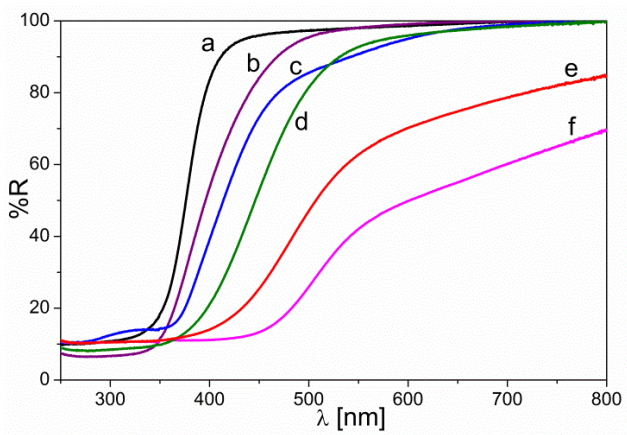

Fig. 4 Absorption spectra of a) TiO_2, b) mechanical mixture of TiO_2 and CeO_2 1:1, c) CeO_2 d) CT90, e) CT10, f) CT50.

The present results differs from those reported by Coronado et al.[28] concerning CeO_2-TiO_2 materials prepared at low Ce loading and by wet impregnation of a TiO_2 matrix for which the red shift observed with respect to the optical transition of titania is very small. This observation outlines the role of the preparation method in determining the physical properties of mixed oxides. The behaviour of the samples here described may be due to more than one reason. The main one seems to be the formation of cerium titanates, whose presence was directly detected ($Ce_2Ti_2O_7$) by Raman spectroscopy at least in the case of CT50. Pure $Ce_2Ti_2O_7$ (pyrochlore structure) contains Ce^{3+} and Ti^{4+} ions in eightfold and six fold coordination respectively. This compound is a brown solid whose colour is due to the presence of Ce^{3+} ions having one electron in the strongly localized 4f orbitals[47]. In the case of CeO_2 the 4f states lie around the mid of the band gap and are empty in the case of fully oxidized ceria while they are occupied ($4f^1$) when Ce^{3+} are formed in reduced materials. The 4f electron of Ce^{3+} generates a pair of spin-orbit split states ($^2F_{5/2}$ $^2F_{7/2}$).[48] In the more complex case of cerium titanates the situation is similar to that of reduced CeO_2 with 8-coordinated Ce^{3+} ions. The same type of spin-orbit split state can thus be assumed to be present which can absorb visible light via a charge transfer transition from 4f to the empty orbitals of Ti^{4+}.[44] The strong coloration assumed by the mixed samples, (which reaches a maximum in the case of CT50, Fig.4), is assigned to the presence of $Ce_2Ti_2O_7$, even though the presence of minor amounts either of Ce^{3+} containing cerium titanates (Ce_2TiO_5) or of reduced Ce^{3+} ions in the CeO_2 matrix or at the oxide-oxide interface cannot be excluded. Cerium titanates are likely to occur at the interfaces between ceria and titania crystals where their formation, upon solid state reaction during calcination, is more probable. Another form of oxide-oxide interaction is in principle possible when, at the heterojunction between two particles, a charge transfer occurs like in the case reported by Diwald and coworkers for the system ZrO_2-TiO_2[49].

XPS spectroscopy

Photoemission spectra of the Ce 3d and Ti 2p core levels corresponding to the different samples are displayed in figure 5. The Ce 3d photoemission peak undergoes relevant changes as a function of Ce concentration.

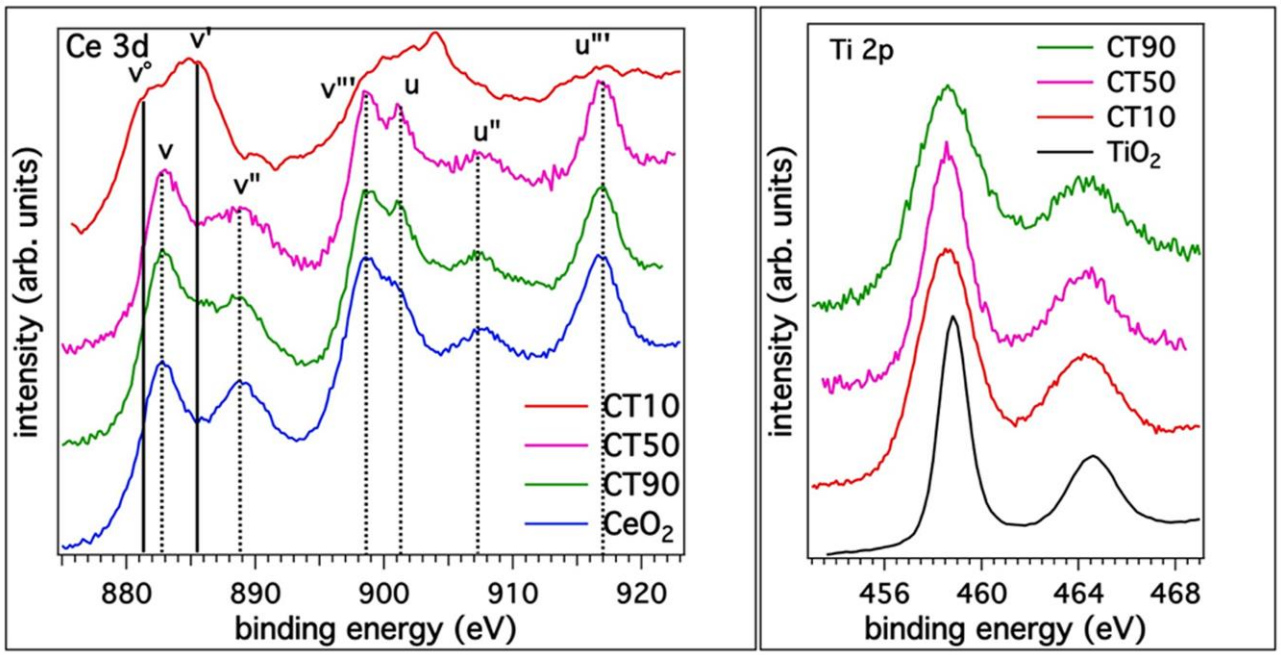

Fig. 5 left: Ce 3d photoemission spectra. The different features due to different final state configuration and oxidation state of ceria are labelled according to literature. v and u components refer to different spin orbit degeneracy, i.e. $3d_{5/2}$ and $3d_{3/2}$ levels, respectively; full lines indicate Ce^{3+} related peaks, while dotted lines are associated to the photoemission from Ce^{4+} ions. Right: evolution of the Ti 2p photoemission spectra as a function of ceria content.

At low Ce content (CT10), the spectrum presents the typical lineshape of Ce^{3+} compounds[50]: two main components can be individuated at 881.2 eV and 885.5 eV, usually referred as v^0 and v' in literature, which are replicated by spin-orbit splitting (18.2 eV) at 899.4 eV and 903.7 eV, respectively[36]. The first peak is related to the emission from Ce 3d states with a Ce $3d^94f^2O2p^5$ final state, while in the second case the hole produced by the photoemission experiments is screened by a $3d^94f^1O2p^6$ state. A very weak feature is also visible at 916.9 eV, (u'''), which is usually used as a qualitative fingerprint of the presence of Ce^{4+} ions and is connected to the poorly screened Ce $3d^94f^0$ O $2p^6$ final state. Therefore the quite distinct structure of the Ce 3d photoemission line indicates the presence of a dominant phase, where Ce is present as Ce^{3+}, and a minority fully oxidized CeO_2 phase.

The existence of ceria in reduced state is well in line with previous photoemission data reported by several authors, either on materials obtained by sol-gel synthesis[2] or wet impregnation[51]. In particular it has been demonstrated that at the interface between ceria and titania Ce^{3+} ions are strongly stabilized thanks to the energy decrease of the Ce 4*f* levels as a result of the mixing with the O 2*p* band of titania[52]. However a role of the size of the nanoparticles (the smaller the particle, the higher the defectivity) influencing the abundance of reduced cerium ions cannot be excluded.

By increasing the amount of ceria (CT50 and CT90), the Ce 3d spectrum becomes very similar to the one of stoichiometric ceria. In the Ce $3d_{5/2}$ peak, the most intense features are the peaks at 882.7 eV (v) and 888.5 eV (v"), which stem from different types of final state screening of Ce^{4+} ions, Ce $3d^94f^2O2p^4$ and Ce $3d^94f^1O2p^5$, respectively. These two features are wider and less sharp than in the CeO_2 reference, indicating the residual presence of the v' component connected to Ce^{3+} species, however, as opposite to the CT10 sample, the u''' satellite is quite intense. We can conclude therefore that despite a prominent presence of oxidized ceria, in the CT50 and CT90 samples there is still the presence of Ce^{3+} ions. Unfortunately, it is not possible to determine if these reduced species are present as interfacial defects or as a $Ce_2Ti_2O_7$ mixed oxide since there is no significant chemical shift between cerium titanate or Ce_2O_3[53] and the co-presence of the predominant CeO_2 phase prevents a reliable separation in chemically shifted components.

It is interesting to note that, despite the presence of Ce^{3+} species in all CT10, CT50 and CT90 samples, their optical absorption is quite different suggesting that not only the compositional also the structural aspects (i.e. formation of an actual cerium titanate) should be taken into account to draw a thorough picture of this advanced material.

The spectrum of Ti 2p core level indicates that titanium is always full oxidized as confirmed by the constant position of the peak maximum at 458.8 eV, which is typical of octahedrally coordinated Ti^{4+} ions[54]. However, it can be noted that the full width at half maximum of the Ti $2p_{3/2}$ peak for the composite is much higher than the reference TiO_2 powder. This can be interpreted as due to the formation of a very intimate composite between the two oxides that determines a variability in the structural environment of Ti^{4+} ions or by the formation of ceria-titania hetero-interfaces characterized by different band bending and consequently small shifts of core level positions.

By means of photoemission we also determined the composition of the different samples as reported in Table 2. The intensity of photoemission spectra has been normalized using the differential cross sections and asymmetry parameters provided by Yeh and Lindau[55] and the inelastic mean free path calculated using the TPP2 algorithm[56].

Table 2 Elemental analysis (molar percentage) of the different samples as determined by photoemission spectroscopy (XPS).

	%O	%Ce	%Ti	%CeO_2[a]
CT10	73.2	6.1	20.7	23
CT50	70.3	18.4	11.3	62
CT90	73.0	25.0	2.0	93

[a] This column reports the Ce molar concentration (in the region explored by XPS) expressed as CeO_2 . This value is directly comparable with the nominal bulk concentration of each sample indicated by the label (10%, 50%, 90%).

As it can be seen from Table 2, the data qualitatively reproduce the trend expected on the basis of the molar ratio used for the preparation, and we do not observe the previously reported enhancing of titanium species in the surface region[2]. At variance, in the subsurface region monitored by photoemission spectroscopy the concentration of Ce is higher (in particular for samples CT10 and CT50) than the stoichiometric value indicating the propensity of Ce component to disperse over TiO_2 crystals. Moreover, oxygen is systematically in excess with respect to the theoretical value (66.6%), probably because of the presence of adsorbed water and hydroxyls.

Surface reactivity with oxygen and EPR spectroscopy.

It is well known that bare CeO_2 easily loses and reincorporates oxygen in reductive and oxidative conditions respectively. This redox cycle occurs in the conditions of the catalytic process. However, simple annealing under vacuum at moderate temperature is sufficient to cause oxygen loss, vacancies formation and excess electron release. When the annealed solid is contacted with oxygen in mild conditions (RT or even lower temperatures) electron transfer occurs with formation of reduced oxygen species including adsorbed O_2^- superoxide ions that are visible in EPR. The chemistry of superoxide adsorbed on ceria has been thoroughly described in a paper by J. Conesa and coworkers[57] who specifically adopt this reactivity as a tool to investigate the surface defectivity of the oxide. We have investigated the reactivity of our CT mixed materials after a mild reduction by annealing 2h at 573 K under vacuum. In these conditions the system behaves similarly to the pure cerium oxide forming surface O_2^- superoxide ions upon adsorption of O_2 onto the annealed samples. Figure 6 compares the EPR spectra of adsorbed O_2^- obtained for CT10, CT50 with that recorded on pure ceria (also prepared via sol-gel).

The spectrum related to ceria (Fig. 6a) shows the typical features already reported for this species[57] with the low field component of the g tensor at g_{zz} = 2.039 (the z direction corresponds to the oxygen internuclear axis) and with an anomalous value of the high field component that, instead of laying around the free spin value (g_e=2.0023) as expected by the ionic model of adsorbed superoxide[58], is at g_{xx}=2.010 and very close to g_{yy} so producing a sort of unresolved perpendicular line. The anomalous value of g_{xx} shown by superoxide ions on cerium dioxide was already discussed[57, 59] in terms of a model involving some degree of covalence in the interaction of adsorbed oxygen with the 4f cerium orbitals and causing deviations from the purely ionic model.

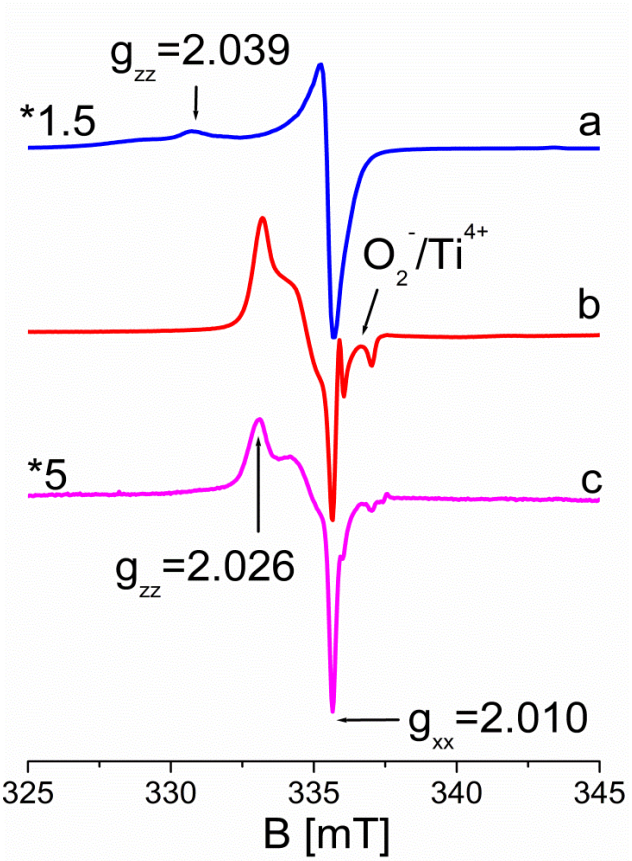

Fig.6 EPR spectra recorded at 77K of superoxide species adsorbed on a) CeO_2, b) CT10, c) CT50 .

Table 3 EPR parameters (g values) of superoxide species.

Centre	g_{zz}	g_{yy}	g_{xx}	Assignment
1	2.039	2.010-2	2.010-2	O_2^- on Ce^{4+} ions (bare oxide)
2	2.027	2.018	2.012	O_2^- on Ce^{4+} ions (mixed oxides)
3	2.027	2.010	2.004	O_2^- on Ti^{4+} ions

The spectra of O_2^- on mixed CT samples have a different lineshape (Fig. 6b and 6c) from that recorded for bare cerium oxide, (Fig. 6a). The spectra in case of mixed materials, in fact, are more symmetric and cover a reduced range of magnetic field. The lowest g component of the signal is the same observed for CeO_2 (g= 2.010) thus suggesting that the adsorption site is a cerium ion also in the case of mixed materials. The low field g component is instead at g_{zz} = 2.026, much lower than that reported on ceria (2.039). The proximity of the three components causes the unusual lineshape of the spectra in figure 6 (b,c).

Furthermore, particularly in the case of CT10, few weak lines due to superoxide on Ti^{4+} ions are also present likely due to spillover of some superoxide from Ce to Ti surface sites because no reduced Ti^{3+} was observed on the sample prior to oxygen adsorption to give reason for a direct electron transfer from Ti to oxygen. This detail confirms the presence of Ti sites at the

surface of the mixed solids. The described spectra are similar to those reported by Coronado et al[28] and obtained on a CeO_2-TiO_2 sample with low cerium loading (0.5%) and prepared by wet impregnation of titania. Similar spectra were also observed by the same Authors on Cl-containing unsupported CeO_2 samples[60].

The spectra of superoxide species adsorbed on mixed CeO_2-TiO_2 oxides in the present work are only partially affected by pumping at room temperature: in these conditions a fraction of superoxide disappears and another one remains adsorbed at the surface producing the spectra in Fig. 6. This residual fraction disappears only if evacuation is performed at T≥373K. This is the main difference between the present case and the spectra reported by the Madrid group on analogous systems[28, 45, 60].

The pronounced differences between the two types of superoxide spectra (bare CeO_2 and mixed materials) prompted us to further investigate the superoxide adducts. The same experiment related to figure 6b was recorded using ^{17}O enriched oxygen in order to observe a hyperfine structure due to the ^{17}O nucleus (nuclear spin I=5/2). Such hyperfine structure (not reported for sake of brevity) indicates the presence of two magnetically equivalent oxygen atoms in the superoxide mojety[58, 61] exactly as observed in the case of pure CeO_2[59]. This points to the presence, also in our case, of a symmetric side-on moiety and excludes the presence of an end-on superoxide adduct capable of rotation around the Ce-O bond (and consequent g values averaging) as it occurs, for instance in the case of surface Co-O_2 species[62].

Summarizing the superoxide species formed by O_2 adsorption on pre-reduced mixed materials (Fig. 6b and 6c) have different g_{zz} values and therefore different spectral profile from those formed on the bare oxide (Fig. 6a and reference [57]).

However both kinds of species are adsorbed onto Ce^{4+} ions and both are symmetrically adsorbed (side-on) on top of the ion. The formation mechanism, despite the non-detectability of the EPR spectrum of Ce^{3+} was already proposed by Conesa and coworkers:

$$Ce^{3+} + O_{2\,(gas)} \rightarrow Ce^{4+}/O_2^- \qquad (1)$$

The reason of the different lineshapes of the two types of superoxide species in figure 6 has therefore to be searched in the different environment of cerium in bare and mixed oxides. This point is the object of further investigation in our group.

Conclusions

Three kinds of CeO_2-TiO_2 mixed oxides in a symmetrical range of compositions and with the molar fraction of each oxide not lower than 0.10 (CT10, CT50, CT90) were prepared in this work. These particular compositions distinguish the solids here investigated from other systems containing a small concentration of ceria dispersed in the TiO_2 matrix previously studied by other authors. The sol-gel method adopted for the preparation originates complex systems whose main features are resumed in the following.

1. The degree of mixing of the two phases is quite high (TEM-EDS) and the less abundant oxide component (cerium oxide in CT10 and titanium oxide in CT90 respectively) tends to disperse on the second phase becoming undetectable by XRD (Fig.1)
2. The two oxide components chemically interact to some extent producing a mixed phase of cerium titanate ($Ce_2Ti_2O_7$, pyrochlore structure). In this compound the cerium is present as Ce^{3+}. The formation of the titanate is highest in the case of CT50. The formation of the titanate is not revealed by X-rays diffraction but is observed by Raman spectroscopy and by optical absorption. The mixed materials in fact exhibit a band gap red shift with respect to the pure oxides (Fig. 4) which causes a pronounced absorption in the visible range. This fact is due to the presence of Ce^{3+} in the stoichiometry of the titanate (pyrochlore structure) which absorbs in the visible, due to the presence of partially populated 4f levels ($4f^1$).
3. The surface of the system is complex and not homogeneous. XPS reveals the presence, in the surface and subsurface layers, of both Ce^{4+} and Ce^{3+} and of Ti^{4+} ions.
4. The mixed solids contacted with oxygen after annealing under vacuum, form superoxide species symmetrically adsorbed onto Ce^{4+} ions (side on). The EPR signal of this species however is markedly different from that of the corresponding species on CeO_2. The reason of such a difference, (which is not due to the structure of the adduct), has to be searched in the particular type of Ce^{4+} adsorbing centers available at the surface of the mixed materials that likely allow a different chemical interaction with oxygen. This topic, which could have a certain relevance for the catalytic properties of the mixed oxides, is currently under investigation in our lab.

Finally, the strong absorption in the visible of the mixed solids (Fig. 4) prompted us to test the photochemical properties of the systems. It was therefore investigated, using a methodology already illustrated in previous work from some of us[63], the presence of photogenerated electrons and holes at the surface of the solid under irradiation with visible light. No trace of photogenerated charge carriers was observed. This indicates that, very likely, the heterogeneity of the system favours a rapid electron-hole recombination. The potential applications of the oxide systems here studied are therefore more in the field of heterogeneous catalysis (where the systems based on cerium have a prominent role) than in that of photocatalysis.

Acknowledgement

This work has been supported by the Italian Ministry of University and Research, MIUR, through the "Programs of National Relevance" (PRIN-2009); the "National Funding for Basic Research" (FIRB) with a project entitled "Oxides at the nanoscale: functionalities and applications" (FIRB RBAP11AYN) and Local Project from University of Torino Id: ORTO11RRT5 "Advances in nanostructured materials and interfaces for key technologies".

Notes and references

[a] *Università degli Studi di Torino, Dipartimento di Chimica and NIS,Via P. Giuria 7, Torino, Italy.*
[b] *Università degli Studi di Padova, Dipartimento di Scienze Chimiche, Via F. Marzolo 1, Padova, Italy.*
[*] *Corresponding author, Fax: +39011670 7855; Tel: +39 011670 7574; E-mail: elio.giamello@unito.it*

1. Z. L. Liu, B. Guo, L. Hong and H. X. Jiang, *J. Phys. Chem. Solids*, 2005, **66**, 161-167.

2. J. Fang, X. Bi, D. Si, Z. Jiang and W. Huang, *Appl. Surf. Sci.*, 2007, **253**, 8952-8961.
3. P. Periyat, K. V. Baiju, P. Mukundan, P. K. Pillai and K. G. K. Warrier, *J. Sol-Gel Sci. Technol.*, 2007, **43**, 299-304.
4. F. Galindo, R. Gomez and M. Aguilar, *J. Mol. Catal. A: Chem.*, 2008, **281**, 119-125.
5. A. Trovarelli and P. Fornasiero, *Catalysis by Ceria and Related Materials: 2nd Edition*, Imperial College Press, London, 2012.
6. J. Kaspar, P. Fornasiero and N. Hickey, *Catal. Today*, 2003, **77**, 419-449.
7. F. Esch, S. Fabris, L. Zhou, T. Montini, C. Africh, P. Fornasiero, G. Comelli and R. Rosei, *Science*, 2005, **309**, 752-755.
8. A. Trovarelli, C. de Leitenburg, M. Boaro and G. Dolcetti, *Catal. Today*, 1999, **50**, 353-367.
9. M. Cargnello, J. J. D. Jaen, J. C. H. Garrido, K. Bakhmutsky, T. Montini, J. J. C. Gamez, R. J. Gorte and P. Fornasiero, *Science*, 2012, **337**, 713-717.
10. S. K. Meher, M. Cargnello, H. Troiani, T. Montini, G. R. Rao and P. Fornasiero, *Appl. Catal. B-Environ.*, 2013, **130**, 121-131.
11. A. L. Camara, M. Monte, A. Martinez-Arias and J. C. Conesa, *Catal. Sci. Technol.*, 2012, **2**, 2436-2439.
12. D. Gamarra, A. L. Camara, M. Monte, S. B. Rasmussen, L. E. Chinchilla, A. B. Hungria, G. Munuera, N. Gyorffy, Z. Schay, V. C. Corberan, J. C. Conesa and A. Martinez-Arias, *Appl. Catal. B-Environ.*, 2013, **130**, 224-238.
13. A. Martinez-Arias, A. B. Hungria, A. Iglesias-Juez, M. Fernandez-Garcia, J. A. Anderson, J. C. Conesa, G. Munuera and J. Soria, *Catal. Today*, 2012, **180**, 81-87.
14. P. Jasinski, T. Suzuki and H. U. Anderson, *Sens. Actuator B-Chem.*, 2003, **95**, 73-77.
15. N. Izu, W. Shin, N. Murayarna and S. Kanzaki, *Sens. Actuator B-Chem.*, 2002, **87**, 95-98.
16. S. D. Park, J. M. Vohs and R. J. Gorte, *Nature*, 2000, **404**, 265-267.
17. A. B. Stambouli and E. Traversa, *Renew. Sust. Energ. Rev.*, 2002, **6**, 433-455.
18. S. Yabe and T. Sato, *J. Solid State Chem.*, 2003, **171**, 7-11.
19. T. Montini, M. A. Banares, N. Hickey, R. Di Monte, P. Fornasiero, J. Kaspar and M. Graziani, *Phys. Chem. Chem. Phys.*, 2004, **6**, 1-3.
20. T. Montini, N. Hickey, P. Fornasiero, M. Graziani, M. A. Banares, M. V. Martinez-Huerta, I. Alessandri and L. E. Depero, *Chem. Mater.*, 2005, **17**, 1157-1166.
21. P. R. Shah, T. Kim, G. Zhou, P. Fornasiero and R. J. Gorte, *Chem. Mater.*, 2006, **18**, 5363-5369.
22. G. R. Bamwenda and H. Arakawa, *J. Mol. Catal. A: Chem.*, 2000, **161**, 105-113.
23. A. L. Linsebigler, G. Q. Lu and J. T. Yates, *Chem. Rev.*, 1995, **95**, 735-758.
24. A. Gallo, T. Montini, M. Marelli, A. Minguzzi, V. Gombac, R. Psaro, P. Fornasiero and V. Dal Santo, *ChemSusChem*, 2012, **5**, 1800-1811.
25. J. C. Conesa, *J. Phys. Chem. C*, 2010, **114**, 22718-22726.
26. A. Hagfeldt and M. Gratzel, *Chem. Rev.*, 1995, **95**, 49-68.
27. N. Serpone and E. Pelizzetti, *Photocatalysis: Fundamentals and Applications*, Wiley & Sons, Chicister, 1989.
28. J. M. Coronado, A. J. Maira, A. Martinez-Arias, J. C. Conesa and J. Soria, *J. Photochem. Photobiol. A-Chem.*, 2002, **150**, 213-221.
29. Q. Z. Yan, X. T. Su, Z. Y. Huang and C. C. Ge, *J. Eur. Ceram. Soc.*, 2006, **26**, 915-921.
30. J. Lin and J. C. Yu, *J. Photochem. Photobiol. A-Chem.*, 1998, **116**, 63-67.
31. A. W. Xu, Y. Gao and H. Q. Liu, *J. Catal.*, 2002, **207**, 151-157.
32. S. W. Chen, J. M. Lee, K. T. Lu, C. W. Pao, J. F. Lee, T. S. Chan and J. M. Chen, *Appl. Phys. Lett.*, 2010, **97**.
33. J. Rynkowski, J. Farbotko, R. Touroude and L. Hilaire, *Appl. Catal. A-Gen.*, 2000, **203**, 335-348.
34. S. Pavasupree, Y. Suzuki, S. Pivsa-Art and S. Yoshikawa, *J. Solid State Chem.*, 2005, **178**, 128-134.
35. T. Lopez, F. Rojas, R. Alexander-Katz, F. Galindo, A. Balankin and A. Buljan, *J. Solid State Chem.*, 2004, **177**, 1873-1885.
36. B. S. Liu, X. J. Zhao, N. Z. Zhang, Q. N. Zhao, X. He and J. Y. Feng, *Surf. Sci.*, 2005, **595**, 203-211.
37. H. Yang, K. Zhang, R. Shi and A. Tang, *J. Am. Ceram. Soc.*, 2007, **90**, 1370-1374.
38. Y.-H. Xu, H.-R. Chen, Z.-X. Zeng and B. Lei, *Appl. Surf. Sci.*, 2006, **252**, 8565-8570.
39. B. Murugan and A. V. Ramaswamy, *J. Phys. Chem. C*, 2008, **112**, 20429-20442.
40. S. Watanabe, X. Ma and C. Song, *J. Phys. Chem. C*, 2009, **113**, 14249-14257.
41. L. Lutterotti, *Nucl. Instrum. Methods Phys. Res., Sect. B*, 2010, **268**, 334-340.
42. A. Adamski, T. Spalek and Z. Sojka, *Res. Chem. Intermed.*, 2003, **29**, 793-804.
43. B. M. Reddy and A. Khan, *Cat. Surv. Asia*, 2005, **9**, 155-171.
44. M. Martos, B. Julian-Lopez, J. Vicente Folgado, E. Cordoncillo and P. Escribano, *Eur. J. Inorg. Chem.*, 2008, 3163-3171.
45. A. Martinez-Arias, M. Fernandez-Garcia, L. N. Salamanca, R. X. Valenzuela, J. C. Conesa and J. Soria, *J. Phys. Chem. B*, 2000, **104**, 4038-4046.
46. M. L. Dos Santos, R. C. Lima, C. S. Riccardi, R. L. Tranquilin, P. R. Bueno, J. A. Varela and E. Longo, *Mater. Lett.*, 2008, **62**, 4509-4511.
47. S. Otsuka-Yao-Matsuo, T. Omata and M. Yoshimura, *J. Alloys Compd.*, 2004, **376**, 262-267.
48. A. Pfau and K. D. Schierbaum, *Surf. Sci.*, 1994, **321**, 71-80.
49. N. Siedl, M. J. Elser, J. Bernardi and O. Diwald, *J. Phys. Chem. C*, 2009, **113**, 15792-15795.
50. P. Burroughs, A. Hamnett, A. F. Orchard and G. Thornton, *J. Chem. Soc., Dalton Trans.*, 1976, 1686-1698.
51. S. Kundu, J. Ciston, S. D. Senanayake, D. A. Arena, E. Fujita, D. Stacchiola, L. Barrio, R. M. Navarro, J. L. G. Fierro and J. A. Rodriguez, *J. Phys. Chem. C*, 2012, **116**, 14062-14070.
52. J. Graciani, J. J. Plata, J. F. Sanz, P. Liu and J. A. Rodriguez, *J. Chem. Phys.*, 2010, **132**.
53. E. Beche, P. Charvin, D. Perarnau, S. Abanades and G. Flamant, *Surf. Interface Anal.*, 2008, **40**, 264-267.
54. V. V. Atuchin, V. G. Kesler, N. V. Pervukhina and Z. Zhang, *J. Electron. Spectrosc. Relat. Phenom.*, 2006, **152**, 18-24.
55. J. J. Yeh and I. Lindau, *At. Data Nucl. Data Tables*, 1985, **32**, 1-155.

56. S. Tanuma, C. J. Powell and D. R. Penn, *Surf. Interface Anal.*, 1993, **20**, 77-89.
57. J. Soria, A. Martinez-Arias and J. C. Conesa, *J. Chem. Soc., Faraday Trans. I*, 1995, **91**, 1669-1678.
58. M. Che and A. J. Tench, *Adv. Catal.*, 1983, **32**, 1-148.
59. M. Che, J. F. J. Kibblewhite, A. J. Tench, M. Dufaux and C. Naccache, *J. Chem. Soc., Faraday Trans. I*, 1973, **69**, 857-863.
60. J. Soria, J. C. Conesa and A. Martinez-Arias, *Colloid Surf. A-Physicochem. Eng. Asp.*, 1999, **158**, 67-74.
61. M. Chiesa, E. Giamello, M. C. Paganini, Z. Sojka and D. M. Murphy, *J. Chem. Phys.*, 2002, **116**, 4266-4274.
62. E. Giamello, Z. Sojka, M. Che and A. Zecchina, *J. Phys. Chem.*, 1986, **90**, 6084-6091.
63. G. Barolo, S. Livraghi, M. Chiesa, M. C. Paganini and E. Giamello, *J. Phys. Chem. C*, 2012, **116**, 20887-20894.